Photoionization of Individual CdSe/CdS Core/Shell Nanocrystals on Silicon with 2-nm Oxide Depends on Surface Band Bending

Oksana Cherniavskaya,[†] Liwei Chen,[†,‡] Mohammad A. Islam,[§] and Louis Brus*,[†]

*Departments of Chemistry and Applied Physics, Columbia University, 3000 Broadway,
MC 3148, New York, New York 10027, and IBM Research Laboratories,
Yorktown Heights, New York*

ABSTRACT

CdSe/CdS nanocrystals are studied by electrostatic force microscopy (EFM) on n- and p-type silicon with 2-nm surface oxide and graphite for comparison. In the absence of above-band-gap excitation, the nanocrystals are not in electrical equilibrium with the substrates. Upon continuous photoexcitation, the particles behave differently on each substrate. On n-type silicon, the particles exhibit predominantly positive charge. However, on p-type silicon, fewer charged particles overall are seen, blinking is more common, and the ratio of negative to positive particles is higher. The low ionization yield on p-Si is apparently due to the fast return of photoexcited electrons that are confined near the silicon/oxide interface by band bending. Nanocrystal photoionization dynamics are sensitive to the state of the silicon across the 2-nm oxide. On graphite, the particles show a greater propensity to oscillate between positive, negative, and neutral states than on the other substrates.

CdSe nanocrystals are a model system for zero-dimensional semiconductor nanostructures and have attracted a lot of attention in the past decade. Their size-tunable electronic properties make them a prime candidate for electrooptical applications. The nanocrystal charge state strongly influences electrical transport properties in photovoltaic and electroluminescent devices, optical gain in nanocrystal lasers,[1,2] and the brightness of nanocrystals in biological luminescence imaging. It has been postulated that single nanocrystal fluorescence "blinking" (i.e., intermittency) and spectral diffusion result from charge redistribution and/or photoionization.[3−9] The kinetics of fluorescence intermittency is complex and implies that a range of quenching states are weakly coupled to the photoexcited internal state, even in single passivated core/shell particles made by the best current synthetic methods.[4,10,11]

In this paper, we report observations of single nanocrystal photoionization using electrostatic force microscopy (EFM). EFM allows the simultaneous mapping of surface topography and electrostatic field gradients[12−15] and provides direct measurements of sample charge and dielectric properties with appropriate modeling. Previously, we have shown that single

CdSe particles on HOPG graphite slowly (ca. 10^{-6} quantum yield) photoionize when excited above their band gap.[16−18] In this study, we investigate the effect of the substrate on the photoionization of CdSe /CdS core/shell nanocrystals. The EFM experiment is quantitatively improved by the use of a recently developed tip−surface capacitive calibration method[19] and by systematically measuring the force dependence upon the height above the surface. We observe substantially different charging behavior on p-type silicon, n-type silicon, and HOPG substrates. The particles have a strong tendency to lose one electron upon photoexcitation; however, negative charge, as well as multiple positive charges per nanocrystal, are observed whereas the equilibrium concentration of positive and negative charges is determined by the substrate type.

CdSe/CdS core/shell passivated nanocrystals have greater stability and a higher fluorescence quantum yield than TOPO-capped particles. It is thought that the outer shell of these particles protects them from photoionization and photooxidation, which would quench luminescence.[20,21] In CdS, overcoated CdSe particles the conduction band offset is small, resulting in a delocalization of the electron wave function over the entire particle while the hole is confined to the core.[9,22] This property should make it easier for electrons to tunnel in and out of the system, compared with the tunneling in ZnS-coated particles in which both the

* To whom all correspondence should be addressed. E-mail: brus@chem.columbia.edu.
  † Department of Chemistry, Columbia University.
  ‡ IBM Research Laboratories.
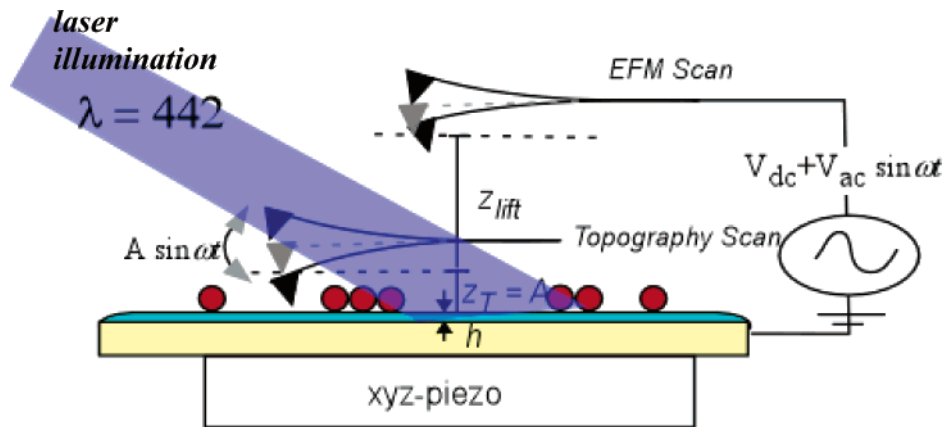 § Department of Applied Physics, Columbia University.

Figure 1. EFM experimental setup.

electron and hole are confined to the core, while still removing surface charge traps, increasing fluorescence yield, and protecting the particle from photooxidation. Thus, it is interesting to investigate the photoionization of these particles.

Core/shell CdSe/CdS nanocrystals (~4.5 nm = ~2-nm CdSe + 2-nm monolayers of CdS + TOPO) used in these experiments were made by organometallic synthesis.[22] They showed an exciton absorption peak in solution at 544 nm with a fwhm of 30.9 nm and a resolved higher exciton at 437 nm. Before deposition onto the substrates, the particles were stored in a solution of hexane and TOPO in a dry atmosphere. The particles were spin-coated onto degenerately doped p-type (B-doped, 0.005−0.01 Ω cm) and n-type (Sb-doped, 0.008−0.03 Ω cm) silicon substrates with a 2-nm thermal oxide layer (obtained from IBM Research, Yorktown Heights, NY). The substrates were cleaned with ethanol and hexane prior to particle deposition. Highly ordered pyrolitic graphite (HOPG) was spin-coated with a thin layer of polyvinylbutyral (PVB) to prevent aggregation because single nanocrystals are highly mobile on graphite.[23,24] The exposure of spun samples to air was minimized typically to no more than 10 min to prevent possible oxidation.[16,18,22] EFM images of photoexcited nanocrystals (grazing angle, HeCd laser (Laconix 200 series), λ = 442 nm, ~0.2 W/cm²) and those exposed only to ambient light were obtained at room temperature in an argon purge box using a Digital Instruments (Santa Barbara, CA) Nanoscope IIIa Multimode AFM with an extender module. Pt−Ir-coated EFM tips (Nanosensors EFM-20) from Molecular Imaging (Phoenix, AZ) were used in all experiments. Their resonance frequency was around 65 kHz, and spring constants were measured to be around 1.35 N/m.

Figure 1 shows the setup for an EFM experiment. A conductive AFM probe is electrically connected to a conductive substrate, forming a capacitor. A tapping-mode topographic scan of the sample is recorded on the first pass of a given line with no bias applied between the surface and the probe. On the second pass, the probe is lifted by a set amount, z_{lift} (Figure 1), and scanned at a constant height above the substrate while a voltage, $V = V_{DC} + V_{AC} \sin(\omega t)$, is applied between them, and the probe is dithered mechanically at its natural frequency. The electrostatic force acting on the probe has the form

$$F_{EFM} = \frac{1}{2}\frac{dC}{dz}V_{tot}^2 + E_z Q_{tip}$$

where $V_{tot} = \varphi + V_{DC} + V_{AC}\sin(\omega t)$ and φ is the contact potential difference between the surface and the probe. The gradient of this force effectively shifts the cantilever's mechanical resonance frequency,[25] ν, by

$$|\Delta\nu| \approx \frac{\nu}{2k}\frac{\partial F_{EFM}}{\partial z}$$

The components of $\Delta\nu$ that oscillate at ω and 2ω are recorded using lock-in detection. During imaging, V_{DC} was set to zero out the contact potential between the substrate and the probe. Thus, there is no DC electric field between the tip and substrate. Such static fields, if present, can polarize substrates and have been used to image Si doping profiles.[26] By using previously reported models, the tip−surface interaction can be interpreted quantitatively.[19] The details of the charge calculation methodology will be reported elsewhere.

Figure 2a shows the images of surface topography, polarizability ($\partial F_{2\omega}/\partial z$), and charge ($\partial F_{\omega}/\partial z$) for a sample of CdS-capped CdSe nanocrystals on p-type silicon with a 2-nm layer of thermally grown oxide. The particles in this Figure are exposed only to room light and the below-band-gap 670-nm diode laser that tracks the AFM cantilever motion. Most of the particles are uncharged; only 2 particles out of about 100 appear to carry charge—one positive (bright) and one negative (dark). Figure 2b shows the same sample area as in Figure 2a within ~15 min of the 442-nm laser being turned on. In this first image, more charged particles appear. Some of the charged particles are circled to show the correspondence between the three images.

Some of the particles appear to be blinking on and off on a time scale of one line scan of the image (~1 s), which can be seen by an increase in the positive signal over nanocrystals that fluctuates from line to line whereas others maintain their state over longer time periods. The number of charged particles does not vary much with laser exposure time after
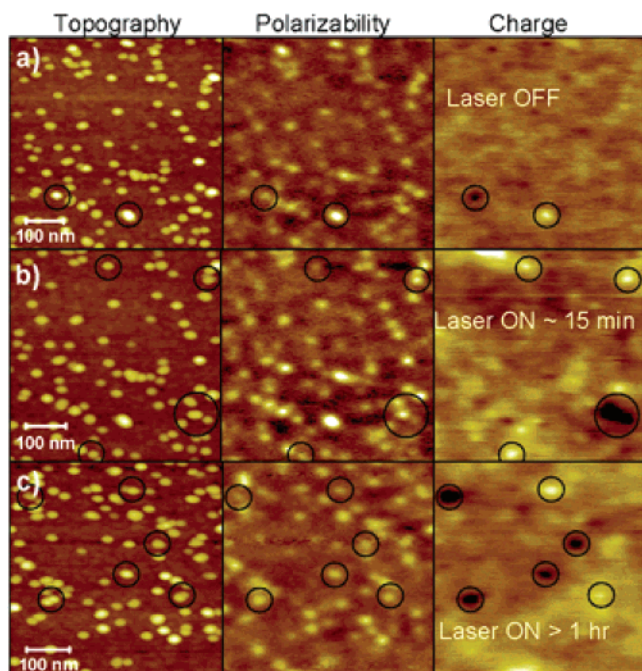
Figure 2. (a) Topography, polarizability, and charge images of CdSe/CdS nanocrystals on p-type silicon. In this image, the sample is exposed only to room light and the AFM laser diode (670 nm). (b) First EFM image of the same area as that in a taken after the sample was exposed to a 442-nm laser. (c) EFM image of a different area of the same sample after the sample had been photoexposed for more than 1 h. The charge images in a, b, and c are plotted on the same scale range. Circles show the correspondence of the charge signal to the nanoparticle in the topography and capacitance images.

Figure 3. (a) Topography, polarizability, and charge images of CdSe/CdS nanocrystals on n-type silicon. In this image, the sample is exposed only to room light and the AFM laser diode. (b) First EFM image of the same area as that in a taken after the sample was exposed to a 432-nm laser. Particle A is negatively charged, and particles B remain neutral. The charge images in a and b are plotted on the same scale.

the first image. After more than 1 h of exposure, the overall charge profile for the area in Figure 2a and b does not show much change. Figure 2c shows a slightly different spot of the same sample with slightly more negative particles to demonstrate that overall there is only a slight preference in these nanocrystals on this substrate to acquire positive rather than negative charge. Given the absorption cross section of CdSe nanocrystals of $\sigma \approx 10^{-15}$ cm^2 and the laser intensity of $\sim$200 mW/cm^2, this should result in $\sim$450 excitations per second. The time it takes for the sample to reach its equilibrium charge state is less than the time it takes to acquire one image, 12 min. This gives us a lower bound on the probability of photoionization of $\sim$4 $\times$ 10^{-5} per excitation.

The behavior of particles on n-type silicon under illumination is very different. Figure 3 shows two sets of EFM images from more or less the same area (3b is slightly zoomed out compared to 3a; a square marks a distinguishing spot on both images). In Figure 3a, the particles are exposed only to room light and the AFM photodiode and are mostly neutral. In Figure 3b, the particles are photoexcited; almost immediately after laser exposure, almost all of the particles acquire a strong, persistent positive charge. In contrast to the sample on p-type substrates, only a couple of particles remain neutral (particles labeled B) or become negative (particle A). The overall charge profile is consistent throughout the substrate and does not change with laser exposure time after the first image. The particles do not show much charge intermittency compared to those on a p-type substrate above.
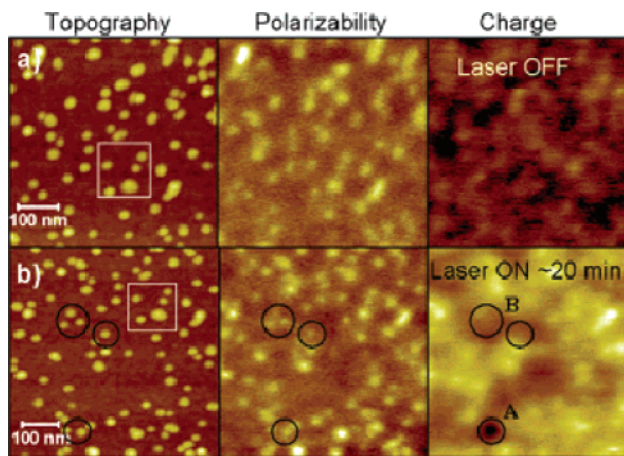
The CdSe particles behave somewhat differently on graphite than on either n- or p-type silicon. Three sets of EFM images of approximately the same area at different times in the experiment are shown in Figure 4. In Figure 4a, the sample had not yet been exposed to 442-nm light. In contrast to the silicon substrates, many of the particles exhibit some partial negative charge; none appear positive. A thin layer ($<$1 nm thick) of PVB was spin-coated onto the graphite before the particles were deposited to prevent aggregation. It may, however, contain some holes or be thin enough that the particle can interact with the tail of the HOPG electron charge tail that extends 5−10 Å above the graphite. Even without net charge transfer between HOPG and the nanocrystals, if the nanocrystal overlaps the HOPG electronic wave function tail, then the local work function is changed, which appears as a static electric field in the ω data.[27] The magnitude of this observed signal is not enough to be due to a full electron transfer and corresponds roughly to an $\sim$250 D dipole pointing out of the plane of the substrate. A local electric field of $\sim$10^5 V/cm would be required to induce such a dipole in a 5-nm CdSe/CdS nanocrystal. When the particles photoionize, this signal changes by the field due to one electron as compared to the dark state.

When the particles are photoexcited, they are charged within the first image as shown in Figure 4b. However, compared to the images taken on both types of silicon substrates, these images show pronounced streakiness that is reminiscent of photoluminescence (PL) blinking,[3,4,6,28] on the time scale of a single line scan. This behavior can be easily observed by looking at particles labeled A and C as well as many others in Figure 4 b and c. It is also common to see particles blinking from positive to negative (particle B) or from negative to neutral (particle D); this type of behavior has not been previously reported.

TOPO-capped particles showed somewhat different results on the n- and p-type silicon substrates but behaved similarly on graphite to CdS-capped nanocrystals. These particles did
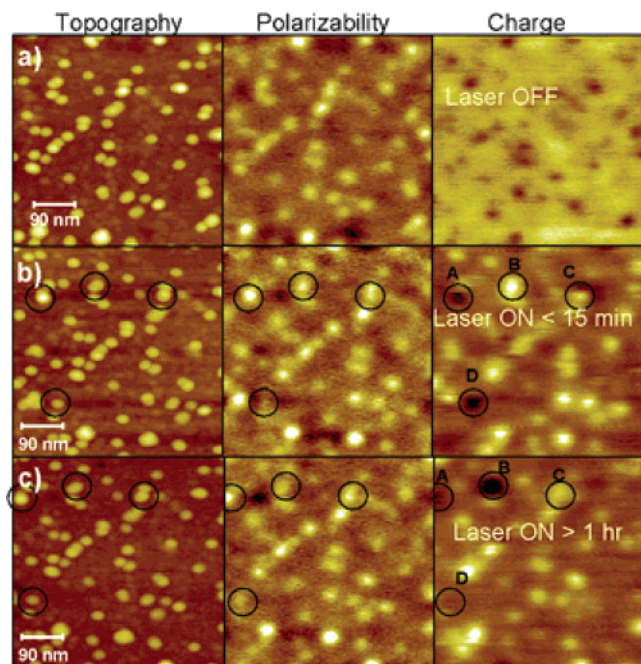
Figure 4. (a) Topography, polarizability, and charge images of CdSe/CdS nanocrystals on HOPG graphite with a thin coat (<1 nm) of PVB. In this image, the sample is exposed only to room light and the AFM laser diode (670 nm). (b) First EFM image of the same area as that in a taken after the sample was exposed to the 432-nm laser. (c) EFM image of the same area of the same sample after the sample had been photoexposed for more than 1 h. Particles A and C are blinking on and off rapidly. Particle B changes from positive to negative, and particle D changes from negative to neutral between images b and c. The charge images in a, b, and c are plotted on approximately the same scale. In a, the scale is shifted up for better contrast, but the range remains the same.

not photoionize to any appreciable extent on p-type silicon and took several hours to reach equilibrium on n-type silicon.

Under ca. 0.2 W/cm^2 (low power) illumination at 442 nm, CdSe/CdS particles photoionize at a rate faster than the ca. 10-min image frame scan time of our experiment on all substrates investigated. On silicon substrates, but not on HOPG, they photoionize much faster than TOPO-capped particles. Both positive and negative charging was observed. For all substrates, the average charge computed for a photoexcited nanocrystal was 1e, with a standard deviation of 0.5e. There are about 10 out of 300 observations when the calculated charge on a nanocrystal is greater than 1.7e. This suggests that there are rare events when a particle loses two electrons. These have been observed on n-type silicon at very small tip−surface separations and only for at most two images for any given particle, which suggests that the electric field from the nearby tip may be responsible for ejecting a second electron from the particle. The presence of the tip, however, is not necessary for photoionization. The observed charging behavior was the same when the nanocrystals were irradiated with the tip away from the surface and then imaged with the laser turned off.

The laser penetration depth in silicon is ~5 × 10^2 nm at 442 nm and ~2 × 10^3 nm at 670 nm. Control experiments at 442 nm on blank silicon substrates showed neither a change in the silicon work function nor a charge buildup in the oxide at ~200 mW/cm^2 excitation used in these experi-
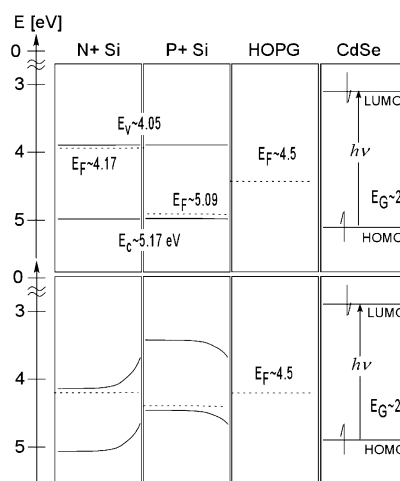

Figure 5. Approximate energy-level diagrams for n-type silicon, p-type silicon, HOPG, and CdSe nanocrystals: (a) flat-band approximation and (b) incorporating band bending at the Si/SiO$_2$ interface due to dangling-bond states.

ments. In addition, the 670-nm radiation of the AFM photodiode does not cause nanocrystal photoionization. We assign the observed nanocrystal charging at 442 nm to direct above-band-gap photoionization.

The substrate has an effect on the probability of acquiring charge as well as on the relative concentration of the observed sign of the charge. This charging process is fully reversible; however, the particles discharge much more slowly than they charge. Independent of the substrate and particle type, it takes on the order of ca. 5 h for the samples to return to the preexposure state.

Figure 5 shows relative energy-band diagrams with (b) and without (a) possible band bending at the Si/SiO$_2$ interface. The relative Fermi-level energies of the substrates would dictate that at electrical equilibrium the particles should acquire predominantly negative charge on n-type silicon and positive charge on p-type silicon; the likelihood of acquiring either charge would be approximately equivalent on graphite. However, this is not observed.

Dangling-bond defects at the silicon/oxide interface can act as electron acceptors or donors depending on the doping type and amount. This creates upward or downward band bending in the n- and p-type silicon, respectively (Figure 5b) and causes Fermi-level pinning at the surface.[29−31] Evidence for this is that the experimental work-function difference between the two substrates is substantially lower (on the order of 300 meV) than would be expected for flat-band degenerately doped n- and p-type silicon (~1 eV). We hypothesize below that this band bending influences photoionization by controlling the concentration of photogenerated electrons at the Si/SiO$_2$ interface

To understand this, first consider ionized nanocrystals after illumination is terminated. They could reneutralize by resonant electron tunneling from occupied Si valence-band states across the oxide to the hole in the nanocrystal HOMO. This process is negligibly slow experimentally (ca. 5-h time scale). On n-type Si, they might alternately reneutralize by transferring Si conduction-band electrons to CdSe. This process is also negligibly slow, perhaps in part because the

band bending of ∼0.3 eV reduces the surface concentration of free electrons by 2 to 3 orders of magnitude from the bulk value.

Yet under illumination we *do* observe electron transfer in the opposite direction, from the optically populated nanocrystal LUMO state to Si through the oxide. The LUMO wave function is delocalized over the whole particle whereas the hole is confined to the core.[9,22,32] Since the spatial overlap of the oxide with the LUMO is better than with the HOMO, the electron transfer from the photoexcited nanocrystal to the substrate is a more probable event. The slow reneutralization is consistent with the poor spatial overlap of the HOMO with the substrate.

Why do we see more positive charging on n-Si? On n-Si, photoelectrons from the nanocrystal are accelerated away from the interface into the Si bulk, and their interface concentration under illumination is small despite the fact that the material is n-type in the bulk. On p-type, the reverse situation holds—the static internal band-bending field keeps photoinjected electrons near the surface in a thin accumulation layer at a net higher concentration than occurs under thermal equilibrium in the dark. We suggest that the fast return of these photoelectrons during illumination reneutralizes nanocrystals, causing blinking, and prevents complete ionization on p-Si. This fast return must compete favorably with recombination with p-Si interior holes. Note also that neutral nanocrystals have electron affinities of ca. 3 eV; they can act as deep electron traps. Some negatively charged CdSe nanocrystals are observed on p-type Si apparently because of fast electron transfer from Si.

Whether this mechanism is correct can be answered only by further experiments as a function of oxide thickness and band-bending depth. Our data do teach us that adsorbed photoexcited CdSe/CdS core−shell nanocrystals with surface TOPO ligands exchange electrons with crystalline Si through 2 nm of oxide. Also, without illumination, the nanocrystals are not in dynamic electrical equilibrium with the substrates: ionized nanocrystals remain ionized, and neutral nancrystals remain neutral on a time scale of hours.

Photoionization on Si is faster with the surface CdS passivation layer than without. This would seem to imply that it is the directly excited internal LUMO "exciton" state that photoionizes rather than a trap state on the nanocrystal surface. Particles without a surface ZnS or CdS layer are known to have much shorter exciton lifetimes because of carrier trapping on the nanocrystal surface.[33−35]

Not all nanocrystals on a given substrate exhibit the same average behavior, as is evident from Figures 2−4. Some turn on and off, some carry only positive charge, some carry negative charge, and some never carry any charge. This variability, as well as the p- and n-type systematic differences above, shows that nanocrystal photoionization is sensitive to many aspects of the local environment such as various trap states in the substrate, local variations in the thickness of the dielectric, the quality of the individual particles, and the state of nearby particles. The preliminary results presented here provide new evidence that it may ultimately be possible to control the photoionization processes in these particles to suit a desired application.

References

(1) Malko, A. V.; Mikhailovsky, A. A.; Petruska, M. A.; Hollingsworth, J. A.; Htoon, H.; Bawendi, M. G.; Klimov, V. I. *Appl. Phys. Lett.* **2002**, *81*, 1303.
(2) Mikhailovsky, A. A.; Malko, A. V.; Hollingsworth, J. A.; Bawendi, M. G.; Klimov, V. I. *Appl. Phys. Lett.* **2002**, *80*, 2380.
(3) Nirmal, M.; Dabbousi, B. O.; Bawendi, M. G.; Macklin, J. J.; Trautman, J. K.; Harris, T. D.; Brus, L. E. *Nature (London)* **1996**, *383*, 802.
(4) Shimizu, K. T.; Neuhauser, R. G.; Leatherdale, C. A.; Empedocles, S. A.; Woo, W. K.; Bawendi, M. G. *Phys. Rev. B* **2001**, *6320*, 205316.
(5) Neuhauser, R. G.; Shimizu, K. T.; Woo, W. K.; Empedocles, S. A.; Bawendi, M. G. *Phys. Rev. Lett.* **2000**, *85*, 3301.
(6) Empedocles, S. A.; Neuhauser, R.; Shimizu, K.; Bawendi, M. G. *Adv. Mater.* **1999**, *11*, 1243.
(7) Empedocles, S.; Bawendi, M. *Acc. Chem. Res.* **1999**, *32*, 389.
(8) Empedocles, S. A.; Bawendi, M. G. *Science (Washington, D.C.)* **1997**, *278*, 2114.
(9) Banin, U.; Brucher, M.; Alivisatos, A. P.; Ha, T.; Weiss, S.; Chemla, D. S. *J. Chem. Phys.* **1999**, *110*, 1195.
(10) Woo, W. K.; Shimizu, K. T.; Jarosz, M. V.; Neuhauser, R. G.; Leatherdale, C. A.; Rubner, M. A.; Bawendi, M. G. *Adv. Mater.* **2002**, *14*, 1068.
(11) Morgan, N. Y.; Leatherdale, C. A.; Drndic, M.; Jarosz, M. V.; Kastner, M. A.; Bawendi, M. *Phys. Rev. B* **2002**, *66*, art. no.
(12) Martin, Y.; Williams, C. C.; Wickramasinghe, H. K. *J. Appl. Phys.* **1987**, *61*, 4723.
(13) Martin, Y.; Abraham, D. W.; Wickramasinghe, H. K. *Appl. Phys. Lett.* **1988**, *52*, 1103.
(14) Nonnenmacher, M.; O'Boyle, M. P.; Wickramasinghe, H. K. *Appl. Phys. Lett.* **1991**, *58*, 2921.
(15) Schonenberger, C.; Alvarado, S. F. *Phys. Rev. Lett.* **1990**, *65*, 3162.
(16) Krauss, T. D.; Brus, L. E. *Mater. Sci. Eng., B* **2000**, *69−70*, 289.
(17) Krauss, T. D.; Brus, L. E. *Phys. Rev. Lett.* **1999**, *83*, 4840.
(18) Krauss, T. D.; O'Brien, S.; Brus, L. E. *J. Phys. Chem. B* **2001**, *105*, 1725.
(19) Cherniavskaya, O.; Chen, L.; Weng, V.; Yuditsky, L.; Brus, L. E. *J. Phys. Chem. B* **2003**, *107*, 1525.
(20) Reiss, P.; Bleuse, J.; Pron, A. *Nano Lett.* **2002**, *2*, 781.
(21) Ebenstein, Y.; Mokari, T.; Banin, U. *Appl. Phys. Lett.* **2002**, *80*, 4033.
(22) Peng, X. G.; Schlamp, M. C.; Kadavanich, A. V.; Alivisatos, A. P. *J. Am. Chem. Soc.* **1997**, *119*, 7019.
(23) Tang, J.; Ge, G. L.; Brus, L. E. *J. Phys. Chem. B* **2002**, *106*, 5653.
(24) Ge, G. L.; Brus, L. E. *Nano Lett.* **2001**, *1*, 219.
(25) Albrecht, T. R.; Grutter, P.; Horne, D.; Rugar, D. *J. Appl. Phys.* **1991**, *69*, 668.
(26) Nelson, M. W.; Schroeder, R. S.; Parkinson, B. A. *J. Vac. Sci. Technol., B* **1999**, *17*, 1354.
(27) Ishii, H.; Sugiyama, K.; Ito, E.; Seki, K. *Adv. Mater.* **1999**, *11*, 605.
(28) Nirmal, M.; Norris, D. J.; Kuno, M.; Bawendi, M. G.; Efros, A. L.; Rosen, M. *Phys. Rev. Lett.* **1995**, *75*, 3728.
(29) Sze, S. M. *Physics of Semiconductor Devices*; Wiley: New York, 1981.
(30) Kronik, L.; Shpira, Y. *Surf. Interface Anal.* **2001**, *31*, 594.
(31) Monch, W. *Semiconductor Surfaces and Interfaces*; Springer: Berlin, 1995.
(32) Nirmal, M.; Brus, L. *Acc. Chem. Res.* **1999**, *32*, 407.
(33) Klimov, V. I.; Mikhailovsky, A. A.; McBranch, D. W.; Leatherdale, C. A.; Bawendi, M. G. *Phys. Rev. B* **2000**, *61*, R13349.
(34) Klimov, V. I.; McBranch, D. W.; Leatherdale, C. A.; Bawendi, M. G. *Phys. Rev. B* **1999**, *60*, 13740.
(35) Shim, M.; Shilov, S. V.; Braiman, M. S.; Guyot-Sionnest, P. *J. Phys. Chem. B* **2000**, *104*, 1494.

NL0340529